

Phase-matched high-order harmonic generation in the nonadiabatic limit

M. Geissler, G. Tempea, and T. Brabec*

Institut für Photonik, Technische Universität Wien, Gusshausstrasse 27/387, A-1040 Wien, Austria

(Received 2 March 2000; published 17 August 2000)

Our calculations show that nonadiabatic effects dominate phase-matched high-order harmonic generation with few cycle laser pulses. The nonadiabatic behavior is a direct consequence of the large ionization rate realized with few-cycle laser pulses, which introduces a nonlinear growth of the harmonic phase with propagation distance. The deviation from linear growth has two striking consequences. On the one hand the nonadiabatic effect drastically reduces the efficiency of conventional phase-matching mechanisms, such as quasi-phase-matching, and on the other hand, it is responsible for a novel phase-matching mechanism, termed nonadiabatic self-phase-matching that is predicted to make high-order harmonic generation in the x-ray regime possible.

PACS number(s): 42.65.Ky, 41.50.+h, 42.50.Hz, 42.65.Re

I. INTRODUCTION

Although the optimization of high-order harmonic generation (HHG) has made rapid progress during recent years [1–3], the efficiency is still too low for many potential applications. The two major limitations of HHG are absorption losses [4,5] and free electron induced dephasing [6–9]. Laser pulse duration and harmonic wavelength determine which of the two mechanisms presents the dominant limitation. Whereas control of the absorption losses is an unsolved problem up to now, there exist a number of proposals for the realization of phase matching [10–14] and experimental demonstrations in the wavelength range above 10 nm [5,15–17].

All previous studies of phase-matched HHG, such as phase matching in a plasma waveguide [10], phase matching by difference frequency mixing [11], quasi-phase-matching [12–15], and phase matching by using the contribution of bound electrons to the refractive index [16,17], have one thing in common. They are based on the “adiabatic” approximation that the change of the free electron density during one optical cycle may be neglected. Under this assumption the phase mismatch grows linearly with propagation distance, and perfect phase matching may be achieved. Throughout this paper, schemes relying on this approximation are referred to as adiabatic phase-matching mechanisms. As HHG is inextricably linked to ionization, the adiabatic assumption is never exactly fulfilled. The variation of the free electron density during an optical period strongly increases with decreasing pulse duration. As a result, ultrashort laser pulses experience subcycle modifications of the laser field, which in turn lead to a nonlinear change of the harmonic phase with propagation distance [18]. These “nonadiabatic” effects [19–21] do not play a role in the long wavelength regime of HHG, where the absorption losses present the dominant limitation to phase-matched harmonic growth [4,5]. However, in the sub-10-nm range, where absorption losses are negligible, nonadiabatic effects determine

the efficiency of phase-matched HHG and may no longer be neglected.

The goal of this article is the theoretical analysis of the influence of nonadiabatic effects on phase-matched HHG. Our calculations reveal two major results.

(i) The nonadiabatic and adiabatic phase contributions are opposite in sign and can compensate, resulting in phase-matched growth. We have dubbed this mechanism nonadiabatic self-phase-matching (NSPM) [18]. Our calculations predict that NSPM enhances HHG above 1 keV by four orders of magnitude thus making HHG in the soft x-ray regime possible. In order to estimate absolute photon numbers our calculations are adjusted by a constant factor obtained from a comparison to experiments [3]. The corrected calculations predict that HHG in helium with 1 kHz, 5 fs Ti:sapphire pulses and a peak intensity of the order of 10^{16} W/cm² will yield $\approx 10^4$ photons/s at a photon energy of 1.5 keV in a 5% bandwidth.

(ii) As a representative of adiabatic phase-matching mechanisms we investigate quasi-phase-matching (QPM) in a periodic gas-vacuum structure. It should be stressed that the conclusions derived from our numerical analysis do not depend on the choice of a particular mechanism, but apply to adiabatic phase-matching schemes in general. We find that the nonadiabatic behavior drastically reduces the efficiency of conventional (adiabatic) phase-matching mechanisms.

Finally, our calculations indicate a surprising trend. In the absence of adiabatic phase-matching mechanisms, the maximum harmonic yield in the sub-10-nm wavelength regime is achieved with few-cycle driver pulses. This maximum harmonic yield cannot be further increased by applying an additional adiabatic phase-matching mechanism. Our finding is a direct consequence of the presence of nonadiabatic effects, which on the one hand limit the efficiency of adiabatic phase-matching schemes and on the other hand are responsible for NSPM.

II. THEORETICAL MODEL

HHG in an atomic ensemble is modeled by a solution of the coupled propagation equations for the fundamental and harmonic fields in one space dimension. The nonlinear evo-

*FAX: +43 1 58801-38799. Email address: brabec@tuwien.ac.at

lution equation for the fundamental field in an ionizing medium in Gaussian units is given by [22]

$$\partial_{\xi} E_l(\xi, \tau) = -\frac{1}{2c} \int_{-\infty}^{\tau} \omega_p^2(\xi, \tau') E_l(\xi, \tau') d\tau' - \frac{2\pi I_p}{c} \frac{\partial_{\tau} n(\xi, \tau)}{E_l(\xi, \tau)}, \quad (1)$$

where the moving coordinate frame $\xi = z$ and $\tau = t - z/c$ was introduced, $\partial_{\xi}, \partial_{\tau}$ represent the respective partial derivatives, and t is the time. The electric field E_l is assumed to propagate in the z direction and to be polarized in the x direction. Further, $\omega_p^2(\tau) = 4\pi e^2 n(\tau)/m$ is the plasma frequency squared at time τ , c is the vacuum velocity of light, e is the electron charge, m is the electron mass, and I_p is the atomic ionization potential. The density of electrons set free by tunnel ionization is determined by

$$n(\xi, \tau) = n_0 \left[1 - \exp\left(-\int_{-\infty}^{\tau} d\tau' w\{E(\xi, \tau')\}\right) \right] \quad (2)$$

with n_0 the initial density of neutral atoms. The ionization rate w is calculated by using the exact static ionization rates given in Ref. [23]. The generation and evolution of high-order harmonic radiation is governed by the wave equation (in Gaussian units)

$$\partial_{\xi} E_h(\xi, \tau) = -\frac{2\pi}{c} \partial_{\tau} D[E_l(\xi, \tau)], \quad (3)$$

where E_h denotes the electric field of the high-order harmonic radiation. In the wavelength regime investigated here, absorption losses experienced by the harmonic radiation are small and may be neglected [5]. The atomic dipole moment for HHG is given by $D = n_0 k d + c.c.$, where d is the single-atom dipole moment in atomic units and $k = 2.542 \times 10^{-18}$ esu cm is the conversion factor between atomic and cgs units. The single-atom dipole moment is determined by a generalized Lewenstein model [24–26] and can be expressed as a product of three probability amplitudes,

$$d(\tau) = \sum_{\tau_b} \frac{1}{\sqrt{i}} a_{ion}(\tau_b) a_{pr}(\tau_b, \tau) a_{rec}(\tau). \quad (4)$$

The three probability amplitudes are given by

$$a_{ion}(\tau_b) = \sqrt{\frac{dn(\tau_b)}{d\tau}}, \quad (5)$$

$$a_{pr}(\tau_b, \tau) = \left(\frac{2\pi}{\tau - \tau_b} \right)^{3/2} \frac{(2I_p)^{1/4}}{E_l(\tau_b)} \exp[-iS],$$

$$S(\tau_b, \tau) = \int_{\tau_b}^{\tau} d\tau' \{ [p(\tau_b, \tau) - A_l(\tau')]^2 + I_p \}, \quad (6)$$

$$a_{rec}(\tau) = \frac{p(\tau_b, \tau) - A_l(\tau)}{\{I_p + [p(\tau_b, \tau) - A_l(\tau)]^2\}^{3/2}}, \quad (7)$$

where a_{ion} and a_{rec} are real and a_{pr} is a complex quantity. Further, $n(\tau)$ is the free electron density as given by Eq. (2),

$$p(\tau_b, \tau) = \frac{1}{\tau - \tau_b} \int_{\tau_b}^{\tau} d\tau' A_l(\tau'), \quad (8)$$

and A_l is the vector potential of the fundamental laser field. The three probability amplitudes can be related to the individual processes involved in HHG [27]. The electron is created by tunnel ionization (a_{ion}) at time τ_b , is accelerated in the electric field (a_{pr}), and recombines to the initial state upon return to the parent ion at an instant τ . The instant of creation τ_b as a function of the time τ is determined by the solution of the algebraic equation $p(\tau_b, \tau) - A_l(\tau_b) = 0$. Note that for the calculation of the single-atom dipole moment the full electric field of the laser pulse is used, i.e., the original model [24] is generalized to account for nonadiabatic effects. Further, the original model is also improved by replacing the Keldysh ionization rate with accurate static ionization rates and by allowing for ground-state depletion in Eq. (5) [25].

III. NONADIABATIC SELF-PHASE-MATCHING

To test our model of HHG, in Fig. 1 numerical results are compared to experimental data obtained from the setup described in Ref. [3]. The harmonic spectrum was generated in helium at a pressure of 500 Torr after an interaction length $\xi = 125 \mu\text{m}$ for the following Ti:sapphire laser pulse parameters: full width at half maximum pulse duration $\tau_f \approx 5$ fs, center wavelength $\lambda_0 \approx 800$ nm, peak intensity $I_0 \approx 4 \times 10^{15}$ W/cm², pulse energy 0.3 mJ at a repetition rate of 1 kHz. For these parameters the shortest harmonics were generated so far. Excellent agreement between experiment and theory is obtained, corroborating the reliability of our model.

Plot (i) in Fig. 1(a) reveals a rapid decrease of the harmonic spectrum with increasing order. The wavelength dependence comes from the fact that the maximum spectral intensity of the N th harmonic depends quadratically on the coherence length [8],

$$L = \frac{2\pi c \omega_0}{N \omega_p^2(\tau)} \propto \frac{1}{N n(\tau)}. \quad (9)$$

The strong increase of the free electron density $n(\tau)$ with increasing harmonic order N is mainly responsible for the rapid drop of the harmonic spectrum.

The harmonic spectrum (ii) in Fig. 1(a) corresponds to a higher peak intensity $I_0 = 1.5 \times 10^{16}$ W/cm². In contrast to plot (i), the decrease of harmonic intensity for $N > 300$ is significantly reduced, and the spectrum remains nearly constant at the high energy end, indicating that the coherence length L is no longer a correct measure of the harmonic growth. This anomalous behavior originates from NSPM, which will be explained below in detail. A remarkable consequence of NSPM is that harmonics up to order $N = 1200$ are generated, corresponding to a photon energy close to 2 keV. The efficiency of HHG in the keV regime can be estimated from a comparison of our calculations to experiments.

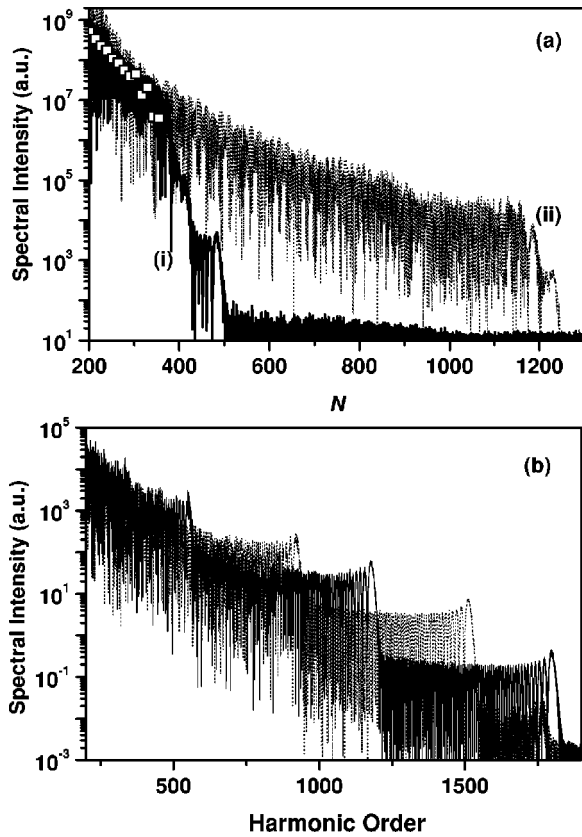


FIG. 1. (a) shows the spectral intensity of harmonic radiation generated in He (500 Torr) versus harmonic order for a Ti:sapphire pulse with $\lambda_0 \approx 0.8 \mu\text{m}$, $\tau_f = 5$ fs, $I_0 = 4 \times 10^{15}$ W/cm², and 0.3 mJ pulse energy at a repetition rate of 1 kHz [plot (i), full line], and $I_0 = 1.5 \times 10^{16}$ W/cm² [plot (ii), dotted line]. The open squares denote the experimentally measured values for the parameters of plot (i). A constant parameter was introduced in the calculations to obtain optimum agreement between experiment and theory. (b) shows the single-atom dipole spectrum for the parameters of plot (ii) in (a) at the entrance of the gas cell (dotted line) and after a propagation distance of 15 μm (full line).

Estimation of the absolute photon number for the experimental data in Fig. 1 yields that $\approx 10^7$ photons/s were generated at the 300th harmonic in a 5% bandwidth [3]. Comparison of the energies contained in a 5% bandwidth of spectra (a) [(b)] at $N = 300$ (1000) in Fig. 1 yields a ratio of $\approx 10^{-3}$ and reveals that $\approx 10^4$ photons/s in a 5% bandwidth at 1.5 keV can be generated.

Figure 1(b) shows the single-atom dipole moment for the parameters of plot (ii) in Fig. 1(a) at the entrance of the gas cell and after a propagation distance of 15 μm . In contrast to the cutoff of the propagated signal, the single-atom dipole moment exhibits several cutoffs at $N = 1800$, $N = 1500$, and $N = 900$, corresponding to electron trajectories returning to the nucleus at the pulse peak, one half cycle before, and two half cycles before the pulse peak, respectively. The first cutoff corresponds to an intensity of 7×10^{15} W/cm², where 98% of the first electron of He is ionized. At such high laser intensities the ionization rate is so strong that, in spite of ground-state depletion, HHG beyond the first cutoff can take place, but with a rapid drop of efficiency between subsequent

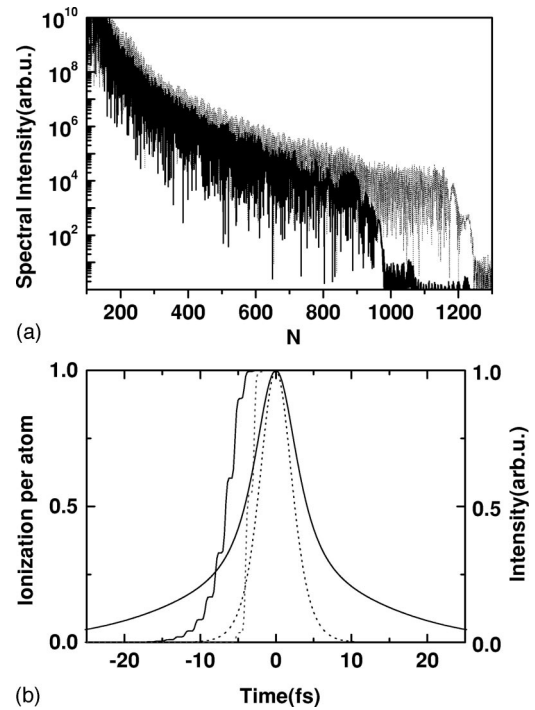


FIG. 2. (a) (Dotted line) harmonic spectrum for the parameters of plot (ii) in Fig. 1(a); (full line) a pedestal is added to the pulse. This is done by adding the electric fields of the initial pulse (dotted line) with $\tau_f = 5$ fs and of a sech pulse pedestal with $\tau_f = 30$ fs. The peak intensity of the combined pulse is again chosen to be $I_0 = 1.5 \times 10^{16}$ W/cm², where the peak intensity of the pedestal is $I_0/10$. The overall full width at half maximum pulse duration $\tau_f = 8$ fs is slightly longer than the duration of the pulse without pedestal. (b) Intensity envelope and relative ionization yield of the pulses without (dotted line) and with (full line) pedestal. The pedestal shifts the ionization curve to lower intensities, reduces the ionization rate, and therewith reduces nonadiabatic effects.

half cycles. The single-atom cutoffs undergo significant shifts during propagation that arise from changes of the laser pulse due to plasma dispersion and nonlinearity. After 15 μm propagation distance the cutoff is shifted from $N = 1500$ to $N = 1200$. For $N = 1250$ (see Fig. 6 below) NSPM does not take place within the first 15 μm , explaining the cutoff found for the propagated signal.

In Fig. 2(a) the harmonic spectrum (dotted line) is plotted for the parameters of plot (ii) in Fig. 1(a), and is compared to the harmonic spectrum (full line) generated by a pulse with a pedestal [see Fig. 2(b)]. At very high peak intensities significant ionization takes place in the pulse pedestal so that the first electron of He is to a great extent ionized before NSPM can take place. This shows that efficient NSPM requires high-quality pump pulses, making cleaning of the leading pulse front necessary.

In Fig. 3 the growth of energy contained in the spectral window between the 950th and the 1000th harmonic is plotted versus interaction length for the parameters of spectrum (ii) in Fig. 1(a). The inset shows the evolution of the harmonic signal over the first micrometer. The harmonic signal grows over the coherence length $L \approx 0.1 \mu\text{m}$, and oscillates for $\xi > L$ between a maximum and a minimum value. For

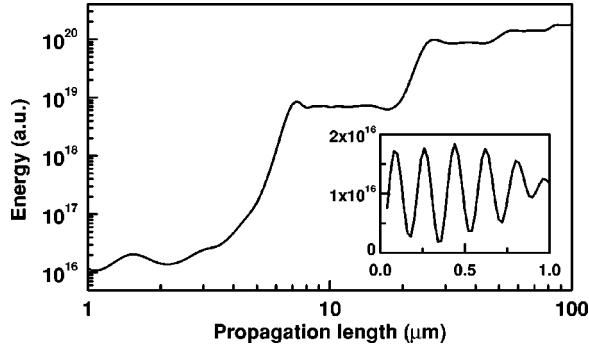


FIG. 3. Energy of the harmonic signal between $N=950$ and $N=1000$ versus propagation distance for the parameters of graph (ii) in Fig. 1(a). The inset shows the growth of the harmonic over the first micrometer.

$\xi \gg L$, NSPM sets in and the harmonic signal exhibits a step-like increase which enhances the energy converted into harmonic radiation by four orders of magnitude. The length over which NSPM occurs is denoted by L_s . During the first step between 4 and 7 μm we find $L_s/L \approx 30$, and the enhancement $(L_s/L)^2 \approx 900$ agrees well with the observed signal growth by three orders of magnitude, indicating the coherent nature of the emitted radiation. Inspection of the temporal profile of the harmonic spectrum between $N=950$ and 1000 shows that during the first 10 μm a single pulse with a duration of 40 as grows. At longer interaction distances the harmonic signal grows at other positions of the laser pulse, which results in the generation of an attosecond pulse train extending over 5 fs.

The calculation in Fig. 3 was repeated for several other spectral windows, peak intensities, pulse durations, and noble gases, from which the following general conclusions can be drawn. As explained above, NSPM does not work close to the single-atom cutoff. Away from the cutoff, where significant ionization takes place, we find that the NSPM induced enhancement, determined by the ratio L_s/L , increases for higher harmonic orders. The reason for this behavior is that L decreases, whereas our calculations show that L_s changes only weakly with increasing N . For example, in Fig. 1 the strongest increase in harmonic efficiency (4–5 orders of magnitude) is observed in the spectral range between $N=800$ and $N=1200$. A comparison of the harmonic range between $N=380$ and $N=400$ for the parameters of plots (i) and (ii) in Fig. 1 shows a NSPM induced enhancement by one order of magnitude (see Fig. 4). This demonstrates that NSPM might also be important for HHG around the water window (2.3–4.4 nm), a spectral range that is very important for x-ray microscopy and holography.

The NSPM induced gain is strongest for peak intensities larger than the saturation intensity of ionization, at which most of the first electron of helium (98%) is ionized ($\approx 7 \times 10^{15} \text{ W/cm}^2$ for a 5 fs Ti:sapphire pulse). In this parameter range the harmonic yield is found to be rather insensitive to variations of the peak intensity, demonstrating that NSPM can take place in a significant volume of the fundamental beam.

The effect of NSPM is strongest for few-cycle laser

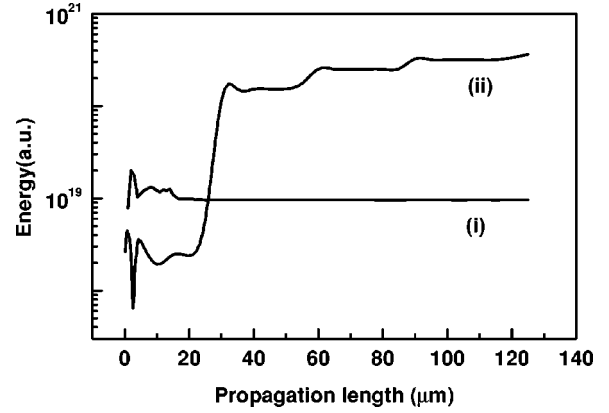


FIG. 4. Energy of the harmonic signal in a 5% bandwidth around $N=400$. Plots (i) and (ii) have been calculated for the parameters of plots (i) and (ii) in Fig. 1(a), respectively.

pulses and decreases rapidly with increasing pulse duration. For a 20 fs pulse with a peak intensity of $1.5 \times 10^{16} \text{ W/cm}^2$ [for the other parameters see graph (b) in Fig. 1], the cutoff of the propagated signal is found to be around $N=500$. The signal generated by the 20 fs pulse between $N=390$ and 410 is enhanced due to NSPM by a factor less than 10.

Calculations for noble gases with lower ionization potentials yield a qualitatively similar behavior to that found in He, demonstrating that NSPM does not depend on a particular atomic species. This opens the possibility of shifting the spectral window where NSPM is most pronounced to lower harmonic orders by using a gas with a lower ionization potential.

In the following, the mechanism for NSPM is identified by investigating the phase growth ϕ_N of a selected harmonic N . Phase-matched growth occurs as long as the harmonic phase does not change, i.e., $d\phi_N/d\xi \approx 0$. A schematic of the laser and harmonic fields generated at two propagation distances ξ_1 and $\xi_2 = \xi_1 + \Delta\xi$ in a frame moving at vacuum light velocity is depicted in Fig. 5. According to the quasiclassical interpretation of HHG [24], the harmonic N is generated by an electron that is created by tunnel ionization at a time τ_b and that recombines to the ground state at an instant τ_r . The evolution of the electron between τ_b and τ_r is determined by the laser electric field. The phase of the harmonic is obtained from a Fourier transform of the atomic dipole moment, as given by Eq. (4), which yields

$$\phi_N = S(\tau_b(\xi), \tau_r(\xi)) - N\omega_0\tau_r(\xi). \quad (10)$$

The quasiclassical action S [24] is determined by the phase change of the electron wave packet (responsible for generation of the N th harmonic) during propagation in the laser field between τ_b and τ_r .

The primary change in ϕ_N results from a shift of τ_r in Eq. (10). The laser field experiences a blueshift of the frequency in the presence of ionization [28]. The resulting phase shift grows linearly with propagation distance. An approximate solution of Eq. (1) in the adiabatic limit yields for the laser pulse phase [8,10]

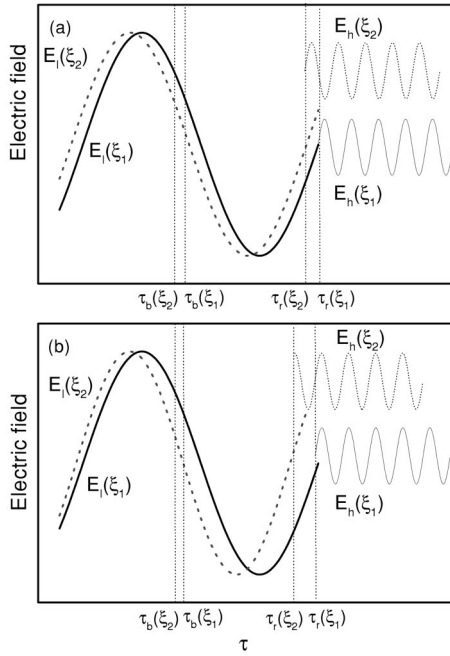


FIG. 5. Schematic of the fundamental field E_l and the harmonic field E_h (generated) at ξ_1 (full lines) and at ξ_2 (dotted lines) in the limits of (a) adiabatic evolution (many-cycle laser pulse) and (b) nonadiabatic evolution (few-cycle laser pulse). The times τ_b and τ_r are the creation and recombination time of the electron that generates a particular harmonic N . The electric fields are plotted in a retarded frame propagating with vacuum light velocity, in which the harmonic field does not change with propagation. The phase difference of harmonics generated at different propagation distances ξ_1 and ξ_2 comes from the ionization induced modification of the fundamental field. In the adiabatic limit (a), the change in free electrons $\Delta n = n(\tau_r) - n(\tau_b) \approx 0$ and the laser field experiences a phase shift that is approximately constant in the time interval between τ_b and τ_r . As the electrons at ξ_1 and ξ_2 experience the same electric field, the phases of the harmonics generated at $\tau_r(\xi_1)$ and at $\tau_r(\xi_2)$ are equal [$S(\xi_2) - S(\xi_1) \approx 0$]. The adiabatic phase mismatch is introduced by a shift of the time $\tau_r(\xi_2) - \tau_r(\xi_1)$ at which the harmonic signal is generated. The nonadiabatic behavior (b) originates from a rapidly changing ionization profile ($\Delta n \neq 0$) causing a sub-cycle variation of the laser electric field. As a consequence, the trajectories of the freed electrons are governed by slightly different electric fields. Therefore, the phases of the harmonic $E_h(\xi_1)$ generated at $\tau_r(\xi_1)$ and of $E_h(\xi_2)$ at $\tau_r(\xi_2)$ are no longer equal. The resulting nonadiabatic harmonic phase change [$S(\xi_2) - S(\xi_1) \neq 0$] is opposite in sign to the adiabatic phase contribution and can cancel it leading to phase-matched growth.

$$\phi_l(\xi) = \frac{\omega_p^2(\tau)\xi}{2c\omega_0}. \quad (11)$$

In the frame propagating at the vacuum speed of light, which is comoving with the harmonic wave, this phase change shifts the time τ_r at which the harmonic is generated to $\tau_r(\xi_2) = \tau_r(\xi_1) + \phi_l(\Delta\xi)/\omega_0$. By virtue of Eq. (10) the shift of τ_r causes a change of the harmonic phase.

In the adiabatic limit of many-cycle pulses the change of free electron density during one laser cycle is negligible; hence $\Delta n = n(\tau_r) - n(\tau_b) \approx 0$. This implies that τ_r and τ_b are

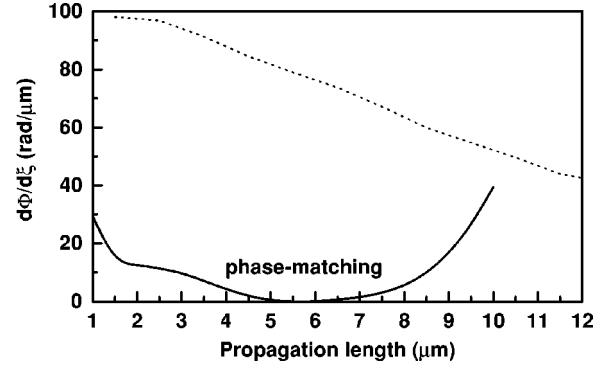


FIG. 6. Evolution of the phase change of the harmonics $N = 975$ (full line) and $N = 1250$ (dotted line) versus propagation distance for the parameters of Fig. 3. The phase change of the harmonic order $N = 975$ is zero exactly at the position at which NSPM takes place in Fig. 3. For the harmonic order $N = 1250$ NSPM does not take place within the first 15 μm . For distances larger than 15 μm NSPM cannot take place, as the single-atom cutoff is shifted below $N = 1250$ [see Fig. 1(b)]. This explains the cutoff position of the propagated harmonic spectrum in Fig. 1.

shifted by the same amount with increasing propagation distance $\Delta\xi$ and that the laser electric field experienced by the electron between τ_r and τ_b remains unchanged, as illustrated in Fig. 5(a). As a consequence, the quasiclassical action S remains constant. Inserting the resulting phase change into the condition $\phi_N(\xi_2) - \phi_N(\xi_1) = N\phi_l = \pi$ yields the coherence length L as given by Eq. (9).

The nonadiabatic behavior originates from a strong sub-cycle variation of the free electron density Δn and from the resulting subcycle changes of the laser electric field. As a consequence, the trajectories of the freed electrons are governed by slightly different electric field evolutions (in time) at different positions along the propagation direction, as illustrated in Fig. 5(b). Therefore, the quasiclassical action S changes with ξ . The nonadiabatic [$S(\xi_2) - S(\xi_1)$] and adiabatic phase changes are opposite in sign, reducing growth of the harmonic phase ϕ_N . For few-cycle laser pulses the nonadiabatic contribution can become strong enough to compensate the adiabatic change of the harmonic phase giving rise to NSPM (see Fig. 6). Between 4 and 7 μm $d\phi_N/d\xi \approx 0$ (for $N = 975$), and NSPM takes place in accordance with Fig. 3.

IV. QUASI-PHASE-MATCHING

We have demonstrated that nonadiabatic effects lead to a deviation from the linear growth of the harmonic phase. Therefore, it must be expected that conventional phase-matching techniques based on the adiabatic assumption are severely limited by the onset of adiabatic behavior. As a representative of adiabatic phase-matching techniques we investigate the QPM scheme depicted in Fig. 7. A periodic gas-vacuum structure is realized by using an array of gas jets. During the interaction of the laser pulse with the gas, harmonic radiation is generated, which is always accompanied by ionization. The presence of the free electrons introduces a phase mismatch between harmonic contributions

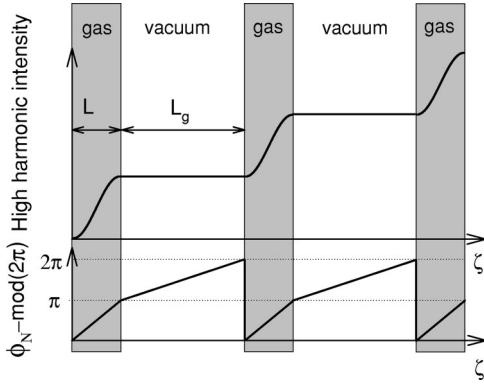


FIG. 7. Schematic of quasi-phase-matching as realized by a periodic gas-vacuum structure. The graphs show the evolution of the intensity and of the phase of a particular harmonic (N), respectively. The harmonic grows coherently in the gas region and reaches a maximum at the (free electron) coherence length L , where dephasing accumulates to a value π . When the length of the vacuum cell is chosen to be the geometric coherence length L_g , the harmonic is brought in phase again so that coherent growth continues in the next gas period.

generated at different propagation distances. As a result, harmonic radiation can grow only over the coherence length given by Eq. (9). In order to achieve QPM, the length of one gas cell is chosen to be equal to $LL_g/(L+L_g)$, where $L_g = \pi z_0/N$ is the geometric coherence length determined by the Gouy phase shift, $z_0 = \pi a_0^2/\lambda_0$ is the confocal parameter, a_0 is the radius of the laser pulse at the beam waist, and λ_0 denotes the center wavelength of the laser pulse. For the sake of simplicity we assume $L_g \gg L$, for which the length of the cell $LL_g/(L+L_g) \approx L$. When the vacuum length is equal to L_g , the Gouy phase shift brings laser and harmonic pulse in phase again, resulting in a continuation of the coherent growth during the next gas cell. The Gouy shift accumulated during vacuum propagation is incorporated into our one-dimensional model by multiplying the laser pulse by a factor $\exp(i \tan^{-1}(L_g/z_0)) \approx \exp[iL_g/z_0]$. The last approximation is valid as long as the interaction length is much shorter than the confocal parameter. This can always be guaranteed by increasing the pulse energy and the beam radius in such a way that the peak intensity remains constant. Finally, the single-atom dipole moment for HHG depends on the pulse intensity, which is changed during propagation due to diffraction. As a result, the phase of the dipole moment decreases in roughly linear proportional to the intensity, with propagation also leading to dephasing [29]. However, this contribution does not scale with the harmonic order and therefore, for higher harmonics can be neglected as compared to free electron induced dephasing.

Limitations of QPM become apparent in Fig. 8, where the harmonic spectrum integrated over a band confined by $N = 430$ and $N = 450$ is plotted versus propagation distance. Graphs (a) and (b) were calculated for a 20fs Ti:sapphire laser pulse ($I_0 = 3.5 \times 10^{15}$ W/cm²) in helium (10 Torr) in the absence and in the presence of QPM, respectively. For these parameters the single-atom cutoff [27] is at $N \approx 445$. In order to compare calculations without and with QPM, the

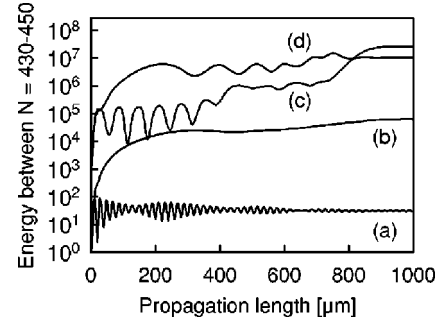


FIG. 8. Growth of the harmonic signal between $N = 430$ and $N = 450$ in the presence (b),(d) and absence (a),(c) of quasi-phase-matching. In order to make a comparison of calculations without and with QPM possible, the vacuum interaction distances were not plotted. Consequently, the distance refers to the length propagated in the gas medium. The radius at the beam waist was assumed to be $a_0 = 0.5$ mm, corresponding to a confocal parameter of $z_0 = 98$ cm. The geometric coherence length of the harmonic $N = 441$ is $L_g = 7$ mm. To relax the pulse energy requirements one could also use smaller confocal parameters for QPM. Calculations were performed for Ti:sapphire laser pulses ($\lambda_0 = 800$ nm) with the following two sets of parameters: $\tau_f = 5$ fs and $I_0 = 6.5 \times 10^{15}$ W/cm² (c),(d); $\tau_f = 20$ fs and $I_0 = 3.5 \times 10^{15}$ W/cm² (a),(b). The helium gas density is 10 Torr, which corresponds to coherence lengths ($N = 441$) of $L = 9.5$ μm and $L = 31.25$ μm for $\tau_f = 5$ fs and 20 fs, respectively.

vacuum interaction distances were not plotted. Plots (c) and (d) refer to HHG with a 5 fs Ti:sapphire laser pulse ($I_0 = 6.5 \times 10^{15}$ W/cm²) without and with QPM, respectively. The peak intensities were chosen to saturate ionization at the pulse peak. Let us first inspect QPM for a 20 fs laser pulse. QPM works properly over the first 350 μm , which corresponds to 35 gas-vacuum periods, and enhances the harmonic yield by approximately three orders of magnitude. This corresponds to a nearly quadratic growth of the harmonic signal. For longer propagation distances nonadiabatic effects start to play a role and the growth is drastically reduced. Our calculations show that the harmonic gain cannot be further increased by using higher laser peak intensities. For 5 fs pulses quasi-phase-matched growth saturates at ≈ 150 μm , corresponding to about seven periodic structures and an increase by a factor of ≈ 50 . In the absence of QPM for $\xi \geq 400$ μm NSPM [18] sets in. Note that the onset of NSPM could be shifted to shorter propagation distances by increasing the gas pressure. In the presence of QPM, NSPM does not work, so that the harmonic gain without and with QPM becomes comparable.

Figure 8 in combination with further calculations for various x-ray and uv wavelengths, for different laser peak intensities and pulse durations, indicates the following conclusions for the sub-10-nm range of HHG. In the absence of phase matching, the use of few-cycle laser pulses is more efficient in the sub-10-nm wavelength regime [8], because the harmonic radiation is created at a lower electron density, resulting in a longer coherence length L . Due to the presence of nonadiabatic limitations, adiabatic phase-matching schemes cannot compensate for the significantly lower efficiency of longer pulses. For few-cycle laser pulses the con-

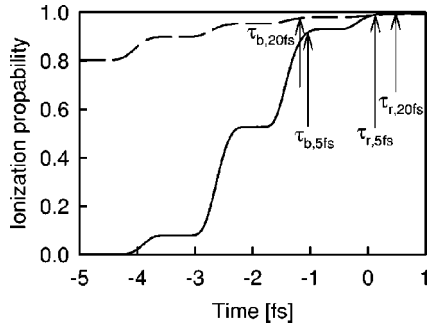


FIG. 9. Ionization profile for 20 fs and 5 fs laser pulses for the parameters of Fig. 8. The arrows indicate the creation (τ_b) and recombination times (τ_r) of the electron, which generates the harmonic order $N=441$ close to the cutoff. The change of the electron density between τ_r and τ_b for the 5 and 20 fs pulses is $\Delta n=0.07$ and $\Delta n=0.015$, respectively; $\Delta n \neq 0$ introduces nonadiabatic effects that result in nonlinear growth of the harmonic phase and limit quasi-phase-matching. For a few-cycle pulse the electron density changes more rapidly than for a multicycle pulse, leading to an earlier saturation of QPM in the case of the 5 fs pulse (see Fig. 8).

tributions of adiabatic phase-matching mechanisms and of NSPM are comparable. As a result, the maximum harmonic yield is obtained by HHG with few-cycle laser pulses. Our calculations indicate that it is not possible to surpass this maximum yield in the sub-10-nm range by applying an adiabatic phase-matching scheme relying on a linear change of the harmonic phase.

Our analysis reveals the limiting influence of nonadiabatic effects on the performance of phase-matched HHG. The adiabatic solution is strictly speaking only valid as long as the laser pulse experiences a constant free electron density, i.e., $\Delta n = n(\tau_r) - n(\tau_b) \approx 0$. This is never the case, as HHG is inextricably linked to ionization. The influence of the nonadiabatic behavior increases with increasing Δn . As the Gouy phase shift introduced during vacuum propagation is linear, it cannot compensate for the nonadiabatic phase contributions in Eq. (10) growing nonlinearly with ξ . As the change in free electron density over one optical cycle increases with decreasing pulse duration, the length over which QPM works is more and more reduced. In Fig. 9 the change of the free electron density is plotted for a 5 fs and a 20 fs pulse. Note that the harmonic $N=441$ is generated in several optical cycles. However, only the electron densities at the times τ_b and τ_r in Fig. 9 fulfill the QPM conditions chosen for the calculations in Fig. 8. The change of the electron density between τ_b and τ_r for the harmonic $N=441$ is found to be a factor of 5 larger for a 5 fs pulse ($\Delta n \approx 0.07$) than for a 20 fs pulse ($\Delta n \approx 0.015$). This explains the fact that in Fig.

8 QPM works for a 20 fs pulse over a five times larger number of gas-vacuum periods than for a 5 fs pulse. Finally, Fig. 9 shows that QPM works best for cutoff harmonics produced in the vicinity of the laser pulse peak, where ionization saturates and Δn is small. For plateau harmonics Δn increases rapidly, which further reduces the maximum gain achievable by QPM. In particular, for few-cycle laser pulses nonadiabatic limitations become so severe that adiabatic phase matching of plateau harmonics does not work at all.

V. CONCLUSION

In this article phase matching of high-order harmonic generation in the nonadiabatic limit was investigated. Our analysis was confined to the sub-10-nm wavelength range, where absorption losses may be neglected. The nonadiabatic evolution of the laser field in the presence of ionization was found to have two effects. (i) It is the source for a self-phase-matching mechanism enhancing high-order harmonic generation with few-cycle laser pulses. Our calculations revealed that as a result of self-phase-matching high-order harmonic generation with photon energies above 1 keV could become possible. Furthermore, although the efficiency of self-phase-matching is reduced for lower harmonic orders, high-order harmonic generation in the water window is still increased by one order of magnitude. Finally, for the experimental realization of keV harmonics very clean pulses are required, as preionization in the leading pulse wings strongly suppresses phase-matched growth. (ii) Nonadiabatic effects limit the efficiency of adiabatic phase-matching mechanisms. In the absence of adiabatic phase matching the highest harmonic yield is achieved with few-cycle laser pulses. As a result of the nonadiabatic effects, this maximum harmonic signal cannot be further increased by applying adiabatic phase-matching schemes. This conclusion is independent of the laser pulse duration used for adiabatic phase matching. Finally, the nonlinear growth of the harmonic phase, ultimately limiting phase-matched high-order harmonic generation, could be overcome by developing a phase-matching scheme that takes account of the nonlinear contributions. One possible realization would be the use of chirped vacuum-gas arrays with a variable length of the gas cells.

ACKNOWLEDGMENTS

The authors gratefully acknowledge the support of Professor A. J. Schmidt and invaluable discussions with F. Krausz. This work was supported by the Austrian Science Fund, Grant No. P12631-PHY, special research program T016, and by the Austrian Nationalbank, Jubiläumsfondsprojekt 7178.

- [1] J. J. Macklin, J. D. Kmetec, and C. L. Gordon III, *Phys. Rev. Lett.* **70**, 766 (1993).
- [2] Z. Chang, A. Rundquist, H. Wang, M. Murnane, and H. C. Kapteyn, *Phys. Rev. Lett.* **79**, 2967 (1997).
- [3] Ch. Spielmann *et al.*, *Science* **278**, 661 (1997).

- [4] E. Constant *et al.*, *Phys. Rev. Lett.* **82**, 1668 (1999).
- [5] M. Schnürer *et al.*, *Phys. Rev. Lett.* **83**, 722 (1999).
- [6] S. C. Rae, K. Burnett, and J. Cooper, *Phys. Rev. A* **50**, 3438 (1994).
- [7] T. Ditmire, K. Kulander, J. K. Crane, H. Nguyen, and M. D.

- Perry, J. Opt. Soc. Am. B **13**, 406 (1996).
- [8] C. Kan, N. H. Burnett, C. Capjack, and R. Rankin, Phys. Rev. Lett. **79**, 2971 (1997).
- [9] Limitations arising from free space propagation of the laser pulse, such as the geometric (Gouy) phase shift, can always be suppressed by increasing the pulse energy and the beam radius so that the peak intensity is kept constant. The geometric coherence length increases with the beam radius squared.
- [10] H. M. Milchberg, C. G. Durfee III, and T. J. McIlrath, Phys. Rev. Lett. **75**, 2494 (1995).
- [11] P. L. Shkolnikov, A. E. Kaplan, and A. Lago, J. Opt. Soc. Am. B **13**, 412 (1996).
- [12] C. Kan, C. E. Capjack, R. Rankin, T. Brabec, and N. H. Burnett, Phys. Rev. A **54**, R1026 (1996).
- [13] J. Peatross, S. Voronov, and I. Prokopovich, Opt. Express **1**, 114 (1997).
- [14] I. P. Christov, H. C. Kapteyn, and M. M. Murnane, Opt. Express **3**, 360 (1998).
- [15] H. R. Lange *et al.*, Phys. Rev. Lett. **81**, 1611 (1998).
- [16] A. Rundquist *et al.*, Science **280**, 1412 (1998).
- [17] Ch. G. Durfee III *et al.*, Phys. Rev. Lett. **83**, 2187 (1999).
- [18] G. Tempea, M. Geissler, and T. Brabec, Phys. Rev. Lett. **84**, 4329 (2000).
- [19] I. P. Christov *et al.*, Phys. Rev. Lett. **77**, 1743 (1996).
- [20] P. Salières, P. Antoine, A. de Bohan, and M. Lewenstein, Phys. Rev. Lett. **81**, 5544 (1998).
- [21] H. J. Shin, D. G. Lee, Y. H. Cha, K. H. Hong, and C. H. Nam, Phys. Rev. Lett. **83**, 2544 (1999).
- [22] M. Geissler *et al.*, Phys. Rev. Lett. **83**, 2930 (1999).
- [23] A. Scrinzi, M. Geissler, and T. Brabec, Phys. Rev. Lett. **83**, 706 (1999).
- [24] M. Lewenstein, Ph. Balcou, M. Yu. Ivanov, Anne L'Huillier, and P. B. Corkum, Phys. Rev. A **49**, 2117 (1994).
- [25] M. Y. Ivanov, T. Brabec, and N. Burnett, Phys. Rev. A **54**, 742 (1996).
- [26] G. Tempea, M. Geissler, and T. Brabec, J. Opt. Soc. Am. B **16**, 669 (1999).
- [27] P. B. Corkum, Phys. Rev. Lett. **71**, 1994 (1993).
- [28] C.-G. Wahlström *et al.*, Phys. Rev. A **48**, 4709 (1993).
- [29] P. Salières, P. Antoine, A. de Bohan, and M. Lewenstein, Phys. Rev. Lett. **74**, 3776 (1995).